Numerical investigation of continuous composite girders strengthened with CFRP

Mohammad A. Samaaneh [1a], Alfarabi M. Sharif [*2],
Mohammed H. Baluch [2b] and Abul K. Azad [2c]

[1] *An-Najah National University, Nablus, Palestine*
[2] *Department of Civil & Environmental Engineering,*
King Fahd University of Petroleum and Minerals, Dhahran, Saudi Arabia

Abstract.   Nonlinear behavior of two-span, continuous composite steel-concrete girders strengthened with Carbon Fiber Reinforced Polymers (CFRP) bonded to the top of concrete slab over the negative moment region was evaluated using a non-linear Finite Element (FE) model in this paper. A three-dimensional FE model of continuous composite girder using commercial software ABAQUS simulated and validated with experimental results. The interfacial regions of the composite girder components were modeled using suitable interface elements. Validation of the proposed numerical model with experimental data confirmed the applicability of this model to predict the loading history, strain level for the different components and concrete-steel relative slip. The FE model captured the different modes of failure for the continuous composite girder either in the concrete slab or at the interfacial region between CFRP sheet and concrete slab. Through a parametric study, the thickness of CFRP sheet and shear connection required to develop full capacity of the continuous composite girder at negative moment zone have been investigated. The FE results showed that the proper thickness of CFRP sheet at negative moment region is a function of the adhesive strength and the positive moment capacity of the composite section. The shear connection required at the negative moment zone depends on CFRP sheet's tensile stress level at ultimate load.

Keywords: continuous span; steel-concrete composite girder; CFRP; Finite Element (FE); contact model

1. Introduction

Composite steel-concrete girders are commonly used in buildings and bridges. For continuous span composite girders, the concrete slab at the negative moment region is neglected or only the longitudinal reinforcement of the slab is considered for composite action. Cracking of concrete slab at negative moment region reduces stiffness and ultimate strength of composite girders. Such cracking may also allow for intrusion by chlorides, leading to insidious corrosion hidden under the finished surface of the structure. Different techniques were deployed to increase the capacity of continuous composite girders. External or internal pre-stressing tendons were used by some

---

∗Corresponding author, Professor, E-mail: fmsharif@kfupm.edu.sa
[a] Assistant Professor, E-mail: m.sanaaneh@najah.edu
[b] Professor, E-mail: mhbaluch@kfupm.edu.sa
[c] Professor, E-mail: akazad@kfupm.edu.sa

researchers to improve the capacity of continuous composite girders Basu *et al*. (1987a, b), Chen *et al*. (2009) and Nie *et al*. (2011). The moment redistribution of continuous composite I-girder with high strength steel was investigated by Joo *et al*. (2015). Experimental and theoretical studies were conducted to find the available and required rotation using plastic analysis. Fang *et al*. (2016) investigated the dynamic characteristics of partially composite continuous girders.

Grace *et al*. (1999), Ashour *et al*. (2004), Lou *et al*. (2015a, b) and Dundar *et al*. (2015) have effectively used the use of CFRP to strengthen continuous Reinforced Concrete (RC) girders. Sharif *et al*. (2015) suggested a new construction approach to maintain the composite action at the negative moment region for continuous composite girders. Experimental testing of continuous composite girders with CFRP sheet bonded to top of concrete slab at negative moment region demonstrated the effectiveness of the new construction approach. However, with the limitations on the numbers of the tested girders, it was not possible to recommend the proper CFRP sheet thickness and length as well as shear connection level at negative moment region.

FE modeling offers attractive, efficient and economical method to investigate behavior of structures. Hawileh *et al*. (2013), Dai *et al*. (2014) and Lou *et al*. (2015a, b) successfully used FE to model RC girders strengthened with CFRP. This paper presents numerical evaluation for continuous composite girders with CFRP bonded to the top of concrete slab at the negative moment region using a FE model developed with commercial software ABAQUS 6.13. This model used to simulate different girders to select the required thickness and length of CFRP needed to develop the full strength of continuous composite steel-concrete girders. The model also used to estimate the required shear connection level to develop full composite action at the negative moment region.

2. Geometry of the modeled girder

A two-span composite steel-concrete girder subjected to a point load at the middle of each span modeled in this study. Four continuous composite girders are used to develop and validate the model as listed in Table 1. Results of experimental testing of these girders presented by (Sharif *et al*. 2015). A control girder prepared without CFRP sheets at the negative moment region (RG) is shown in Fig. 1, whereas the other three girders were strengthened with one, two, and three layers of CFRP bonded to the top of the concrete slab at negative moment region (G1, G2, and G3 respectively) as illustrated in Fig. 2. The thickness of CFRP was the main variable of the study and the length of CFRP chosen in accordance with the ACI specifications (2008) for development length. Shear studs of 19 mm diameter were used to form the composite action between steel beam and concrete slab. The girders were designed to have full composite action at positive and negative moment regions, the shear studs spacing is shown in Fig. 1.

Table 1 List of Girders tested by Sharif *et al*. (2015)

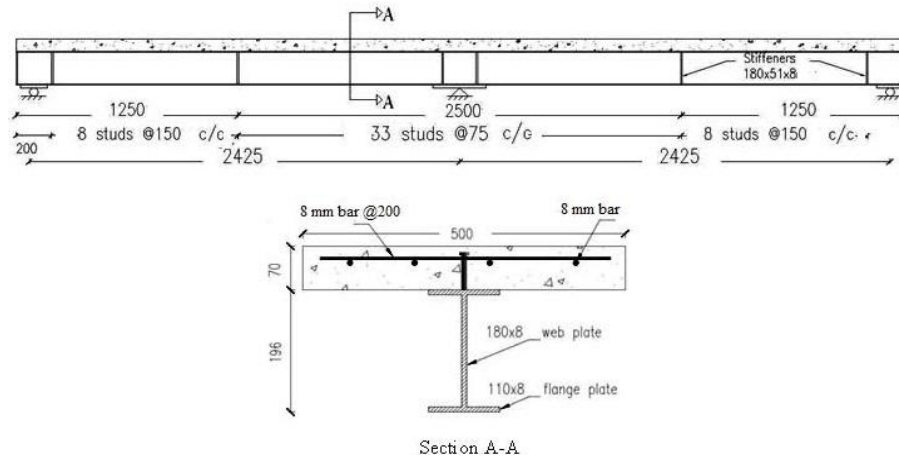| Girder	Number of CFRP layers	Thickness of CFRP (mm)
RG	No CFRP	-
G1	One layer	0.131
G2	Two layers	0.262
G3	Three layers	0.393

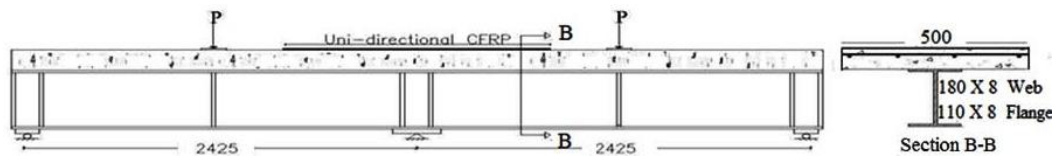Fig. 1 Geometry of control girder and distribution of shear studs (dimensions in mm)

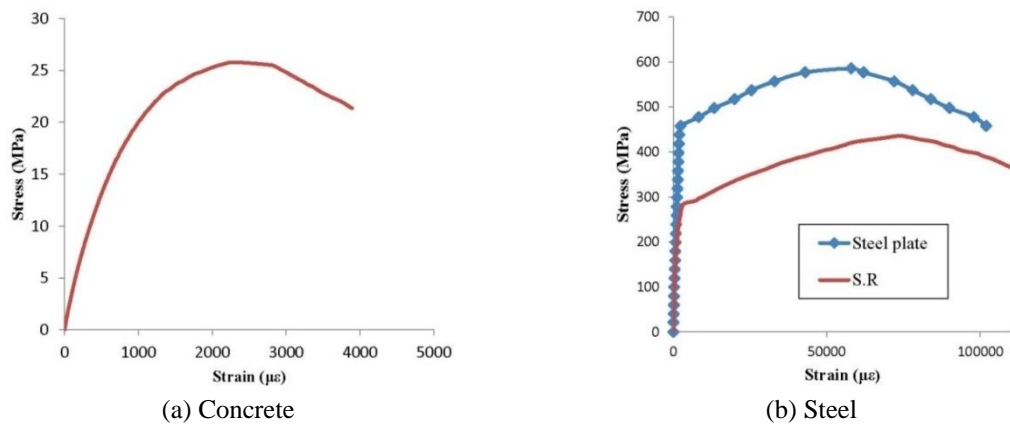Fig. 2 Girders bonded with CFRP at the negative moment region (dimensions in mm)

(a) Concrete   (b) Steel

Fig. 3 Stress-strain diagram

Table 2 Mechanical properties of structural steel and steel reinforcements

	Structural steel	Steel reinforcement
Yield strength (MPa)	278.6	417.7
Ultimate strength (MPa)	430.7	591.3
Poisson ratio	0.29	0.30
Young Modulus (MPa)	205000	205000

Table 3 Mechanical properties of concrete and CFRP

Concrete		CFRP	
Compressive strength (MPa)	26.4	Tensile strength (MPa)	3483
Young Modulus (MPa)	23800	Ultimate strain	0.015
Poisson ratio	0.2	Young Modulus (MPa)	232200
Strain at ultimate	0.0026	Density (gm/cm^3)	1.8
Strain at failure	0.004	Thickness (mm)	0.131
Tensile strength (MPa)	3.1		

The mechanical properties of the composite girder componentsreported by Sharif *et al.* (2015). The stress-strain curves of concrete, steel, and steel reinforcement areshown in Figs. 3(a) and (b) and the mechanical properties are summarized in Tables 2 and 3.

Unidirectional CFRP sheet of 0.131 mm thickness and 500 mm width (Nitowrap FRC grade 230) was used in this study. CFRP properties obtained from the manufacturer summarized in Table 3.

The tensile strength of CFRP σ_u is 3480 MPa and the design ultimate strain is 0.015. Nitowrap primer base and Nitowrap hardener, mixed according to the company evaluated by pull out test. CFRP sheetbonded to concrete block as schematically shown in Fig. 4.

Strain gauges werefixed to CFRP sheet surface to measure slip between concrete block and CFRP sheet according to Bilotta (2010). The adhesive load versus slip curve is shown in Fig. 5(a). The adhesive shear strength is 2.0 MPa and behaved elastically up to 1.4 MPa.

Shear capacity of studs evaluated by two-way push-out test. Steel section with two shear studs at each side cast with concrete as schematically shown in Fig. 6 (Topkaya *et al.* 2004). LVDT (linear variable differential transducer) fixed at bottom of steel section to measure the slip and load applied at top of steel section. The measured load versus slip of shear connectors shown in Fig. 5(b).
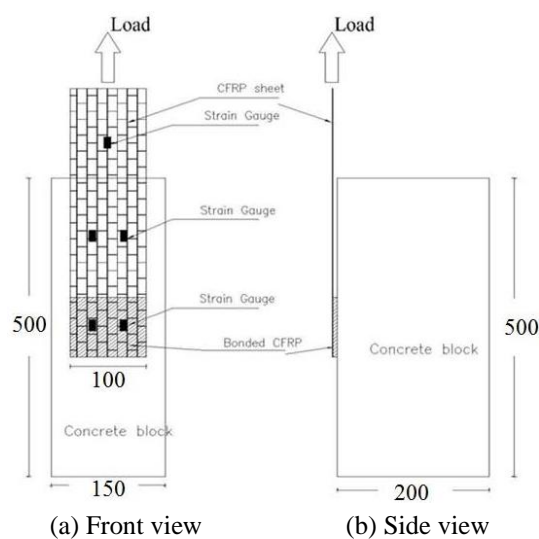

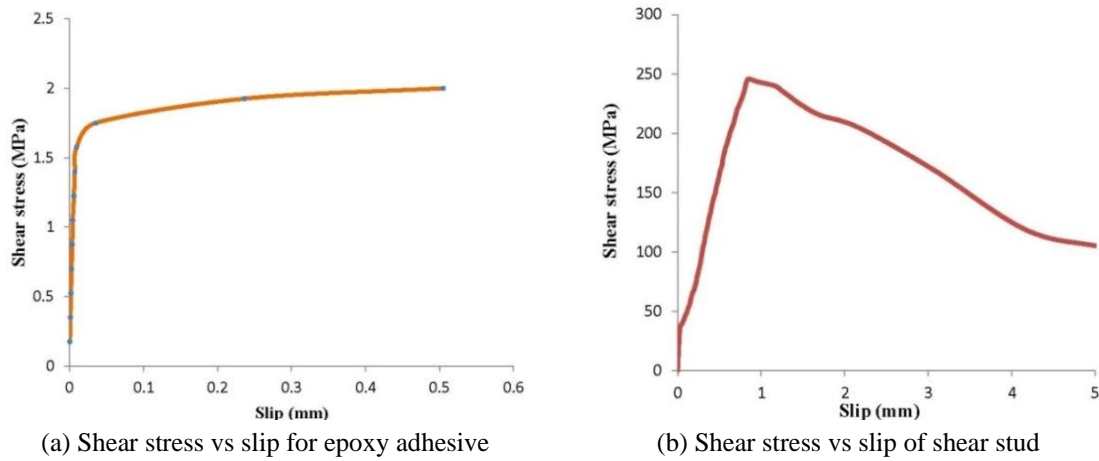Fig. 4 Schematic view for testing epoxy (dimensions in mm)

(a) Shear stress vs slip for epoxy adhesive (b) Shear stress vs slip of shear stud

Fig. 5 Slip characterization of epoxy adhesive and shear studs
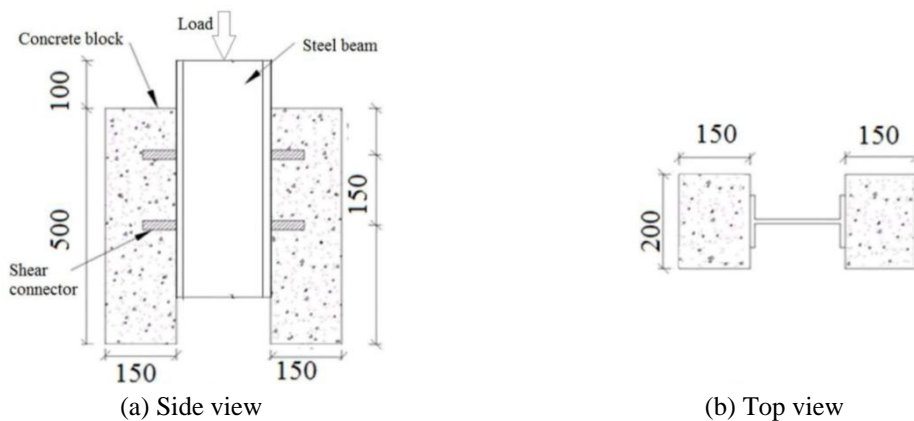

(a) Side view (b) Top view

Fig. 6 Two-way push-out test for shear studs (dimensions in mm)

3. Finite element modelling

The two-span continuous composite girders were modeled using ABAQUS/Explicit solver as shown in Fig. 7. The point loads applied as an equivalent pressure load on 50 mm wide bearing steel plates mounted to top of concrete slab and covering its full width. Two rollers and one pin line restraints were assigned at the mid of bearing plates at the supports. Adequate attention focused on the development of hex-dominated mesh and assigning interaction between various surfaces.

The components of composite girder were meshed using part-by-part basis instead of using global or sweep features. A regular structured hex-dominated mesh generated. Adequate mesh size was adapted to ensure accuracy of results as shown in Fig. 8. Eight-node linear brick element (C3D8R) was used to model the solid elements; concrete, steel, and shear studs. The steel reinforcement modeled as 2-node linear 3-D truss (T3D2) whereas 4-noded shell element (S4R) used to model CFRP.
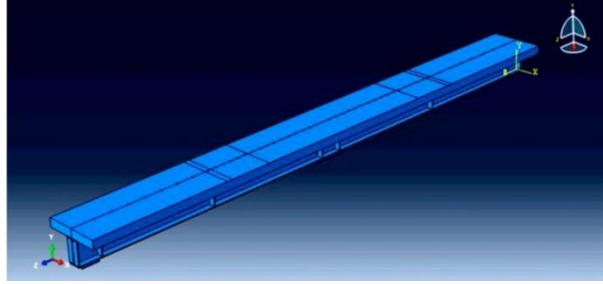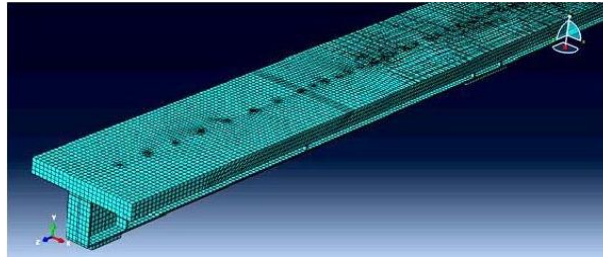
Fig. 7 The modeled girder (dimensions in mm)

Fig. 8 Meshing of girder

4. Modeling of concrete

Concretemodeled using a damage plasticity model as proposed by Lubliner *et al.* (1989) and extended by Lee and Fenves (1998) follows a non-associated flow rule. This model requires as input the stress-inelastic strain of concrete for both compression and tension obtained from uniaxial compression and tension tests. The parameters for the concrete damage plasticity model are given in Table 4.

The concrete elastic-plastic response described using the effective stress $\bar{\sigma}$ and the hardening variables $\dot{\varepsilon}^{pl}$ and $\widetilde{\varepsilon}^{pl}$.

$$\bar{\sigma} = D_o^{el}:(\varepsilon - \varepsilon^{pl}) \in \{\bar{\sigma}|F(\bar{\sigma}, \tilde{\varepsilon}^{pl}) \leq 0\} \tag{1}$$

$$\tilde{\varepsilon}^{pl} = h(\bar{\sigma}, \tilde{\varepsilon}^{pl}).\dot{\varepsilon}^{pl} \tag{2}$$

$$\dot{\varepsilon}pl = \dot{\lambda}\frac{\partial G(\bar{\sigma})}{\partial \bar{\sigma}} \tag{3}$$

F is the yield function and λ a non-negative plastic multiplier and both satisfy the following

Table 4 Concrete damage plasticity parameters

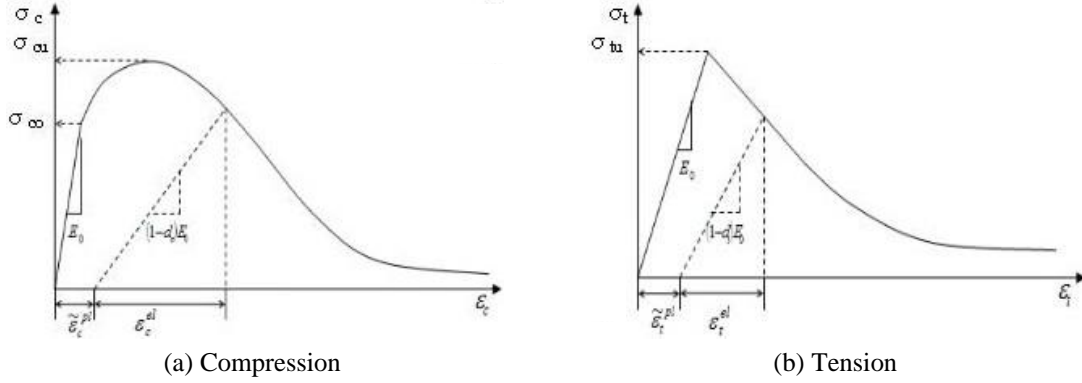| Young modulus	Poisson ratio	Dilatation angle	Eccentricity	f'_{bc}/f'_c	K	Viscosity parameter
23800 MPa	0.2	36	0.1	1.16	0.67	0

(a) Compression   (b) Tension

Fig. 9 Concrete damage model

criteria $\dot{\lambda} F = 0$; $\dot{\lambda} \geq 0$; $F \leq 0$. Plastic flow is controlled by flow potential G. The Cauchy stress tensor σ is calculated in term of the stiffness degradation variable d ($\bar{\sigma}$, $\tilde{\varepsilon}^{pl}$) and the effective stress as $\sigma = (1 - d)\ \bar{\sigma}$.

The elastic modulus of the damaged concrete reduced using stiffness degradation variable d. The hardening and softening of concrete, for both compression and tension, characterized by considering uniaxial loading conditions first and then extended for multi-axial conditions. The concrete specimen is unloaded from any point on the strain-hardening and/or strain softening branch of the uniaxial nonlinear stress-strain curve, the unloading response weakened, due to which the elastic stiffness of the material appears damaged (or degraded) as shown in Fig. 9.

Degradation of the stiffness is significantly different between compression and tension. For both cases, the effect is more considerable as the plastic strain increases. The response of degraded concrete is defined using two independent uniaxial damage variables d_t and d_c as functions of the plastic strains, and field variables. The uniaxial degradation variables modelled as monotonically increasing functions of the equivalent plastic strain. The degradation variables can take values ranging from zero, for the undamaged material, to one, for the fully damaged material. If E_0 is the initial (undamaged) elastic stiffness of the concrete, the stress-strain relation under uniaxial tension and compression loading expressed as

$$\sigma_t = (1 - d_t)E_0 \left(\varepsilon_t - \left(\tilde{\varepsilon}^{pl} \right)_t \right) \tag{4a}$$

$$\sigma_c = (1 - d_c)E_0 \left(\varepsilon_c - \left(\tilde{\varepsilon}^{pl} \right)_c \right) \tag{4b}$$

The effective uniaxial stress in tension $\bar{\sigma}_t$ and compression $\bar{\sigma}_c$ are

$$\bar{\sigma}_t = \frac{\sigma_t}{(1 - d_t)} = E_0 \left(\varepsilon_t - \left(\tilde{\varepsilon}^{pl} \right)_t \right) \tag{5a}$$

$$\bar{\sigma}_c = \frac{\sigma_c}{(1 - d_c)} = E_0 \left(\varepsilon_c - \left(\tilde{\varepsilon}^{pl} \right)_c \right) \tag{5b}$$

The compression damage variable d_c and plastic straincalculated by conducting loading

(a) Uniaxial stress-strain diagram   (b) Uniaxial stress-inelastic strain diagram
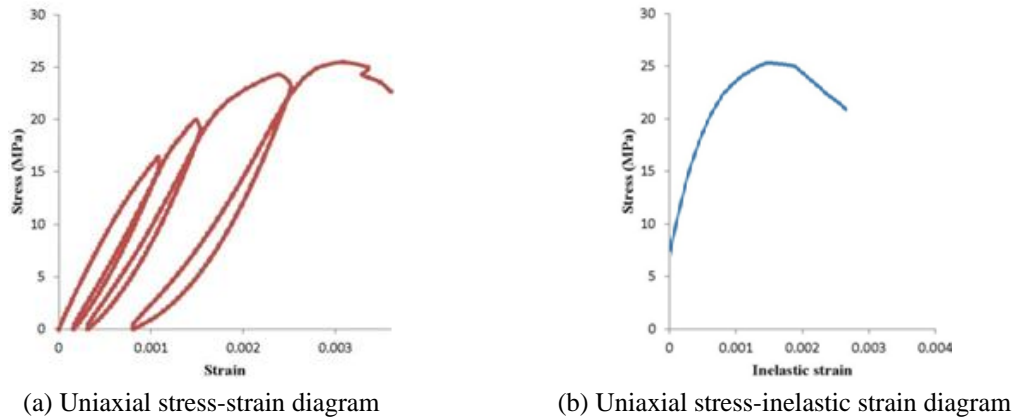
Fig. 10 Loading-unloading uniaxial compression test

unloading uniaxial compression test as shown in Fig. 10(a). The obtained data used to calculate the Inelastic strain (Fig. 10(b)) and to calculate the damage variable using Eq. (4b). Similarly, tension damage variable d_t evaluatedusing Eq. (4a) and Fig. 9(b) takingthe limiting concrete strain at 0.003. At any point on the stiffening part of the curve in Fig. 9(b), get the total stress and strain then unload to evaluate the plastic strain.

5. Modeling of composite girder elements

Structural steel, steel reinforcement and shear studs were modeled using isotropic plasticity model. The stress-plastic strain of steel and steel reinforcement obtained from the stress-strain curves shown in Fig. 3(b), used as input data for the model. The 19 mm diameter and 50 mm length shear studs modeled as solid parts using 3D element having the same material properties as that of steel reinforcement. CFRP sheets modeled as linear elastic composite laminate of 0.131 mm thickness for each layer. The principal material direction of fabric assigned along the girder longitudinal direction.

The mechanical properties for the combined CFRP sheet and adhesive presented in Table 5 are evaluated using equations six to eleven proposed by Mallick (1993).

The elastic moduli for longitudinal and transverse directions E_{11} and E_{22} evaluated from equations six and seven, respectively. The plane shear moduli $G_{12} = G_{13}$ and normal to the plane shear modulus G_{23} evaluated from equations eight and nine, respectively. Poisson ratio v and ultimate tensile strength σ_{co} evaluated from equations ten and eleven, respectively. The elastic modulus of CFRP E_f (232 GPa) and its volume fraction V_f (0.408) are provided by the manufacturer. The individual mechanical properties of CFRP and adhesive used in equations six to eleven are represented values reported by Tauris (2009).

Table 5 Definition of combined CFRP and adhesive parameters in ABAQUS

E_{11} (MPa)	E_{22} (MPa)	Y	G_{12} (MPa)	G_{13} (MPa)	G_{23} (MPa)	σ_{co} (MPa)
97000	5120	0.31	1990	1990	19970	1500

$$E_{11} = E_f V_f + E_a (1 - V_f) \tag{6}$$

$$E_2 = E_f E_a / (E_a V_f + E_f (1 - V_f)) \tag{7}$$

$$G_{12} = G_{13} = G_f G_a / (G_a V_f + G_f (1 - V_f)) \tag{8}$$

$$G_{23} = E_{22} / (2(1 + \upsilon_{23})) \tag{9}$$

$$v = v_f V_f + v_a (1 - V_f) \tag{10}$$

$$\sigma_{co} = V_f \sigma_u + (1 - V_f) E_a / E_f \sigma_u \tag{11}$$

For CFRP, shear modulus $G_f = 98$ GPa and poisons ratio $v_f = 0.2$. For the adhesive, elastic modulus $E_a = 3.1$ GPa, shear modulus $G_a = 1.2$ GPa and poisons ratio $v_a = 0.38$. CFRP stress level was limited to the de-bonding stress evaluated experimentally by Sharif *et al*. (2015).

6. Modeling of interaction

The interfacial regions modeled as surface-surface contacts. Different models of surface contact were used to simulate the interaction of steel-concrete, concrete-CFRP, and stiffeners-steel beam. Mechanical interaction between the stud and concrete surfaces was modeled using friction formulation in tangential direction and hard contact in normal direction to avoid penetration of shear studs. The slope of the linear part of the curve in Fig. 5(b) represents the normal stiffness interaction between shear studs and concrete slab. The penalty method used for tangential behavior using coefficient of friction as 0.2. Studs defined as the master elements, whereas the surrounded concrete considered as slave. Cohesive contact was used to simulate the behavior of adhesive material between concrete and CFRP. The values of normal and tangential stiffness calculated from Fig. 5(a) as the slope of shear stress/unit length with respect to the slip. The calculated tangential stiffness was 4000 MPa. Welding of shear studs, stiffeners and steel bearing plates to the steel beam simulated by tie constraints whereas the reinforcement bars in both directions defined as embedded regions inside concrete.

7. Validation of the model

The FE model is validated using the experimental results (Sharif *et al*. 2015) for the load-deflection curves, strain measurements, concrete slab cracks, and steel-concrete interface slip.

7.1 Load-deflection behavior

The numerical load-deflection curves showed good agreement with the experimental results as shown in Figs. 11(a)-(d). The numerical load-deflection curves simulated the ultimate capacity of the composite girders retrofitted with varying amount of CFRP at the negative moment region, in
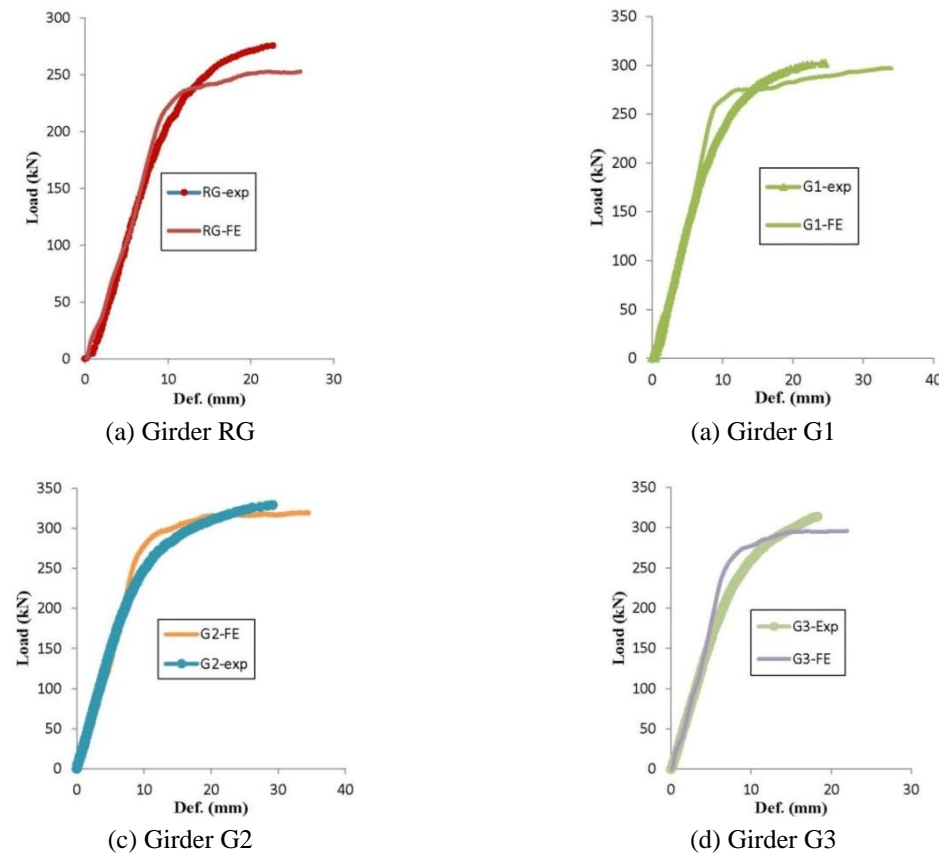
(a) Girder RG

(a) Girder G1

(c) Girder G2

(d) Girder G3

Fig. 11 Comparison between numerical and experimental Load-deflection curve
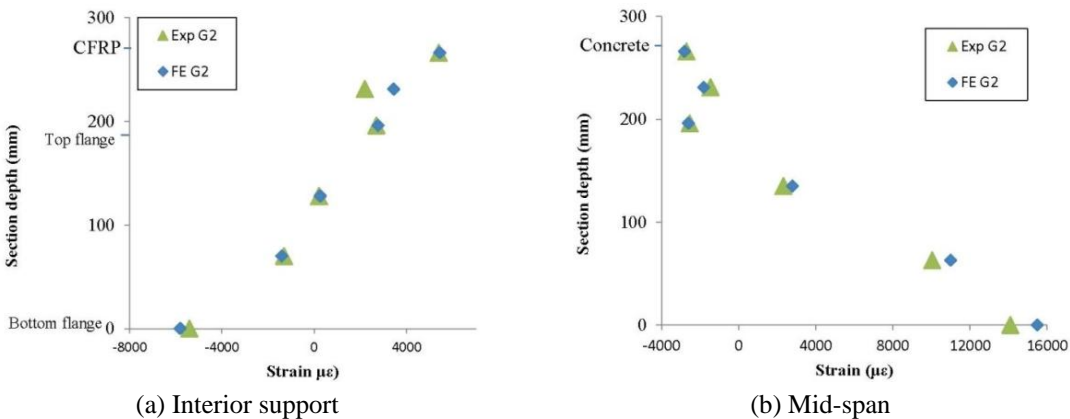

(a) Interior support

(b) Mid-span

Fig. 12 Strain distribution across the depth of girder G2 at ultimate load

addition to capturing various phases of behavior of the composite girders including the yielding of the steel flange section and the girder deflection at failure.

Table 6 Comparison between experimental and numerical stresses at ultimate load at mid-span

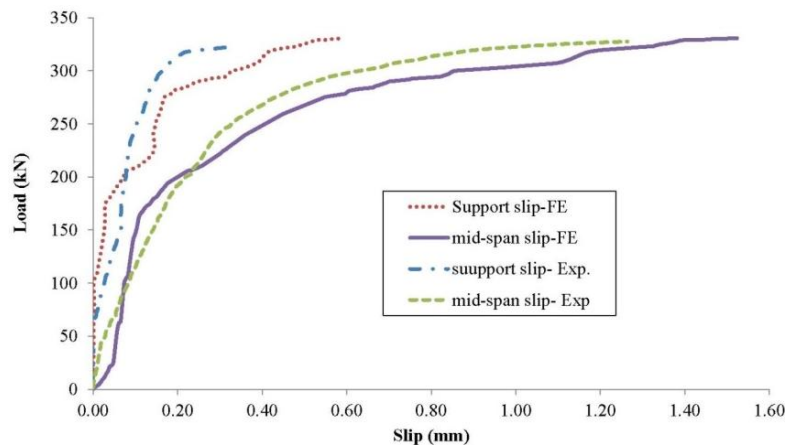| Girder	Stresses at the top of concrete slab (MPa)		Stresses at bottom flange of steel section (MPa)	
	Exp.	Numerical	Exp.	Numerical
RG	22.0	19.1	293	308
G1	21.0	18.8	308	310
G2	24.5	23.1	320	328
G3	22.0	16.8	308	305

Fig. 13 Comparison between experimental and FE steel beam-concrete slip

7.2 Strain measurements

The numerical strain distributions along the cross section showed close agreement to the experimental ones as shown in Figs. 12(a) and (b) for girder G2. The stresses at mid-span for concrete and steel presented in Table 6 for both experimental and numerical results. Numerical stress results are close to the experimental values for all girders.

7.3 Steel-concrete interface slip

Surface-surface contact model was used to model the interface between shear studs and the surrounded concrete. Implementing the contact definition gave the model an ability to predict the relative slip between concrete slab soffit and the top flange steel girder. The comparison of numerical interface slip compared with experimental LVDT's readings at the same locations showed good agreement as shown, as an illustration, in Fig. 13 for girder G2. Comparison between experimental and numerical load-slip curves for girder G2 over the interior support and at mid-span illustrated in Fig. 13.

7.4 Mode of failure and qualitative concrete cracks

All girders experimentally tested failed by shear-compression of concrete slab as shown in Fig. 14. The concrete plastic damage model used in modeling concrete slab was able to capture this
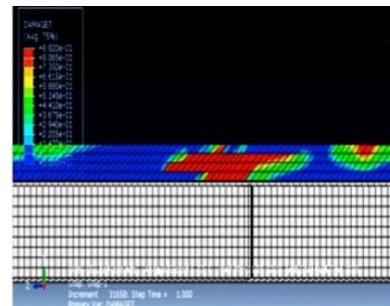
type of failure as illustrated in tension and compression concrete damage shown in Figs. 15(a) and (b). Combination of tension and compression damage of concrete slab at mid-span (Figs. 15(a) and (b)) reflects the actual failure of concrete slab depicted in Fig. 14. Cracks in concrete slab over the interior support shown in Fig. 16 indicating their locations and orientations. The transverse cracks developed longitudinally along shear studs were also captured as shown in Fig. 17. The numerical results showed that the maximum value for the compression damage variable (d_c) is 0.33 whereas

Fig. 14 Shear-compression failure at mid-span region
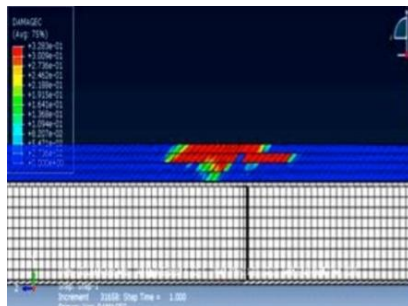
(a) Compression damage d_e at mid-span   (b) Tension damage d_t at mid-span
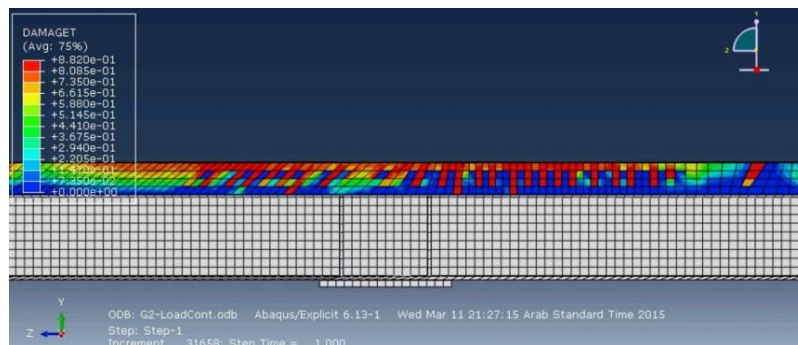
Fig. 15 Concrete damage

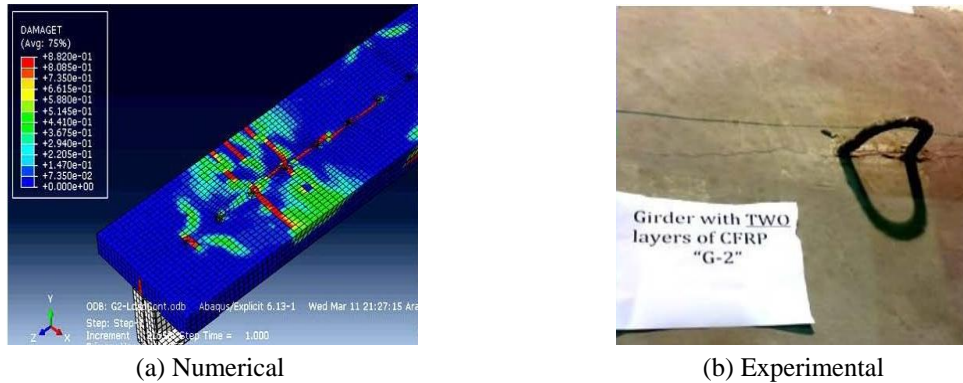Fig. 16 Concrete cracks at negative moment zone at ultimate load

(a) Numerical

(b) Experimental

Fig. 17 Cracks along the line of shear studs at ultimate load

the maximum tension damage variable (d_t) is 0.88. Strain measurements showed that the strain at top of concrete slab at mid-span was close to 0.0026, less than the crushing strain of approximately 0.003. The occurrence of shear-compression failure of concrete slab at mid-span preempted the development of the ultimate moment capacity of girders and hence the ultimate load.

8. Parametric study

A parametric investigation of the three key design parameters namely the thickness and length of CFRP sheet and the degree of shear connectivity at the negative moment region was conducted on girder G2 (the same girder used to validate the model). However, an increased slab thickness of 90 mm used to prevent shear-compression failure of the slab prior to reaching full positive moment capacity. The geometry and material properties of the girder remained unchanged.

8.1 CFRP thickness

Depending upon the used thickness of CFRP sheet, three distinct behavioral failure patterns noted for the continuous composite girder. First, premature de-bonding of CFRP sheets prior to reaching the ultimate load. Second, attainment of the plastic positive moment capacity at mid-span prior to full yielding of the steel section at the negative moment zone. Third, a full yielding of steel section at the negative moment region first followed by the development of plastic positive moment capacity and crushing of concrete slab at mid-span. The third development is the desired one in design, as it provides the best utilization of CFRP and the girder strength.

Of the four girders investigated with different CFRP thicknesses, one was the control girder with no CFRP at negative moment region, marked as CG, and the other three girders, C1, C2, and C3 were strengthened with one, two and three layers of CFRP, respectively. Epoxy adhesive strength taken as 2.0 MPa according to the pullout test. The FE results presented in Table7indicate that girders CG and C1 achieved their full capacities while girders C2 and C3 failed prematurely by de-bonding of CFRP sheet. For both girders, the shear stresses exceeded the epoxy adhesive strength, and therefore de-bonding occurred near the cut-off ends of CFRP sheets. The tensile stress in CFRP at the ultimate load for girders C2 and C3 was lower in comparison to girder C1 due to the adhesive strength limitation as indicated by its stress level in Table 7. Therefore, for this

Table 7 Effect of CFRP thickness on the ultimate capacity of composite girder

Girder	CFRP thickness (mm)	CFRP stress at ultimate load (MPa)	Ratio of moment capacities (α)	Ultimate load (kN)	Type of failure
CG	-	-	1.55	312	Crushing of concrete
C1	0.131	1480 (0.43 σ_u)	1.43	341	Crushing of concrete
C2	0.262	1438 (0.41 σ_u)	Not achieved	354	De-bonding of CFRP
C3	0.393	1003 (0.29 σ_u)	Not achieved	355	De-bonding of CFRP
RC2	0.262	1450 (0.42 σ_u)	1.29	361	Crushing of concrete
RC3	0.393	1510 (0.44 σ_u)	1.20	388	Crushing of concrete
RC4	0.524	1053 (0.31 σ_u)	1.18	385	Crushing of concrete
RC5	0.655	727 (0.21 σ_u)	1.14	375	Crushing of concrete

Table 8 Definition of combined CFRP and Sikadur-30 adhesive parameters in ABAQUS

E_{11} (MPa)	E_{22} (MPa)	v	G_{12} (MPa)	G_{13} (MPa)	G_{23} (MPa)	σ_{co} (MPa)
101000	5780	0.31	2750	2750	23300	1650

girder with the given adhesive property the proper CFRP thickness is 0.131 mm.

As both girders C2 and C3 failed prematurely by de-bonding of CFRP, it was of interest to examine if the load carrying capacity can further enhanced by preventing the failure of epoxy adhesive. A higher shear strength adhesive 4 MPa (Sikadur-30) was used. The mechanical properties of combined CFRP sheet and the new adhesivepresented in Table 8. It is revaluated as previously done using Eqs. (6) to (11) proposed by Mallick (1993).

Four girders RC2, RC3, RC4 and RC5 were modeled using girder CG with different CFRP thicknesses as listed in Table 7 and adhesive strength of 4.0 MPa. The stiffness of girders found to be directly proportional to the thickness of CFRP as illustrated in Fig. 18. The ultimate capacity of the girders increased with the increase of CFRP thickness up to girder RC3 as illustrated in Table 7. CFRP sheet not well utilized for girders RC4 and RC5 as compared to girder RC3. The increase in CFRP thickness for girders RC4 and RC5 increased the ultimate moment capacity close to the positive moment capacity as indicated by the ratio (α), where (α) is the ratio of the plastic moment capacities at positive to negative moment regions in Table7. This caused lesser rotation of the girder at the interior support and failure of girder at mid-span occurred before reaching the moment capacity at moment zone. Consequently, girders RC4 and RC5 recorded a smaller ultimate load than RC3. All girders failed by crushing of concrete slab at positive moment region. The increase of the girder ultimate capacity is a function of both CFRP enhanced capacity of the section at the negative moment region. The increase of CFRP sheet thickness increases the moment capacity at interior support but decreases the ratio α as indicated in Table 7. For a certain CFRP sheet thickness for girders RC4 and RC5, positive moment capacity at mid-span develops prior to negative moment at the interior support, implying underutilization of CFRP as shown in Table 7. The reduction of ultimate strength is due to the partial yielding of steel section at interior support. The numerical results for girders in Table 7 indicate that when the ratio α is less than 1.2, considerable part of the steel section at interior support and CFRP sheet are underutilized. It appears that CFRP thickness for girder RC3 meets the target objective of being adequate to
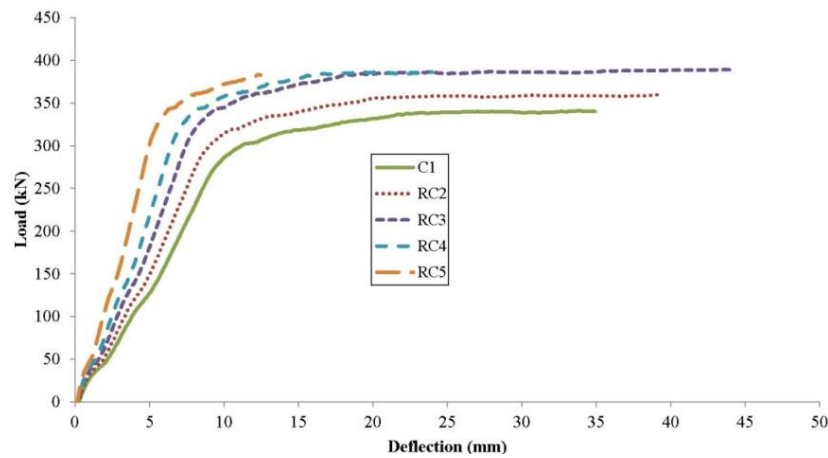
Fig. 18 Load-deflection curves of girders with different thickness of CFRP

(a) Elastic vs plastic moment and the corresponding
     rotation of girder RC3

(b) Elastic vs plastic moment and the corresponding
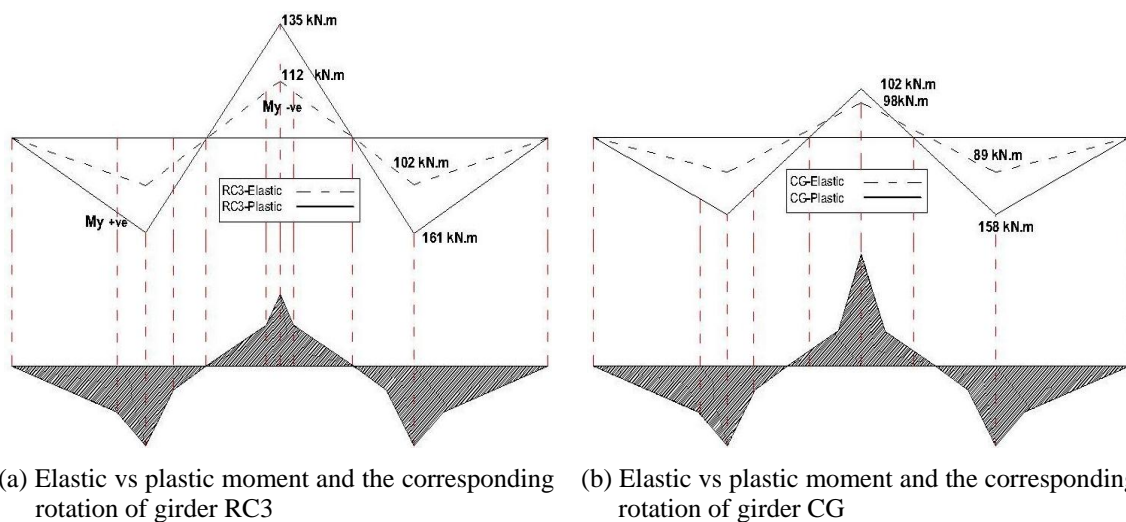   rotation of girder CG

Fig. 19 Elastic vs Plastic moment diagram and the corresponding rotation of girders CG and RG3

develop full moment capacities at the positive and negative moment regions.

The use of CFRP reduces the moment redistribution for the girder. As illustrated in Fig. 19 for girders RC3 and CG, a slight reduction in the rotational capacity (curvature) at negative moment region whereas it allows more curvature at mid-span beyond failure.

8.3 Proper length of CFRP

According to the ACI specifications, CFRP length should extend at least 150 mm from each side of the inflection point, and extra 150 mm for any additional layer of CFRP. Four girders, each with a different length of CFRP sheet, modeled to investigate the minimum required development length of CFRP sheet to reach the ultimate plastic capacity of composite girders: girders L1, L2,
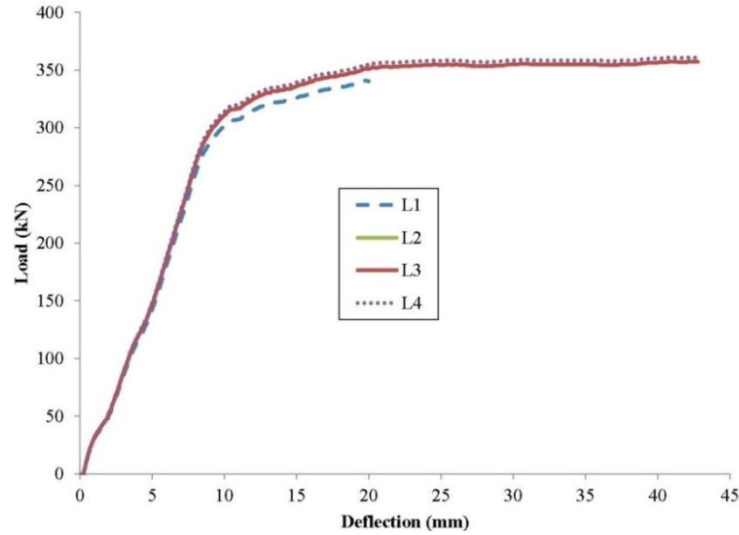
Fig. 20 Load-deflection curves for girders with different CFRP length

L3 and L4 having zero, 100 mm, 200 mm, and 300 mm development length, respectively. The total length of CFRP sheet with zero development length is 1000 mm. All girders modeled had unchanged CFRP sheet thickness of 0.262 mm, concrete slab thickness of 90 mm and adhesive strength of 4.0 MPa.

The ultimate capacity for girders with CFRP development length extended 200 mm or more beyond the inflection point had no effect on the ultimate strength as illustrated in Fig. 20. Reduction of CFRP development length to 100 mm has a slight reduction of ultimate strength from 360 kN to 355 kN. However, the ultimate strength decreased to 338 kN resulted when CFRP terminated at inflection point (i.e., no development length). This reduction in capacity was due to de-bonding of CFRP prior to reaching the ultimate moment capacity of composite girders. Therefore, this confirms the ACI requirements to extend CFRP sheets at least 150 mm from each side.

9. Requirement of shear connection at negative moment zone

The FE model used to simulate the effect of shear studs spacing and investigate the required shear connection level to develop full composite action at negative moment region. Three girders modeled with 75 mm, 120 mm and 150 mm shear studs spacing at the negative moment region. The shear stud spacing of 120 mm represents full composite action between steel section and CFRP sheet stressed at 0.35 of its ultimate capacity as given by Eq. (12)

$$N = \frac{(A_{S.R} f_y + n\, t\, b_f\, 0.35\, \sigma_u) * 2}{Q} \tag{12}$$

N = number of shear studs within the negative moment region, n = number of CFRP layers, t = thickness of CFRP layer, b_f = width of CFRP, Q = shear stud capacity, $A_{S.R}$ = area of steel reinforcement, f_y = yielding stress of steel reinforcement, σ_u = ultimate tensile stress of CFRP. Eq.

(12) developed to meet the requirement of shear connectors to resist the total longitudinal tensile force due to reinforcement yielding and CFRP force.

The shear stud spacing of 75 mm and 150 mm represent over and partial connection, respectively. Shear stud spacing slightly affected the ultimate capacity and stiffness of the composite girders as illustrated in Fig. 21. A negligible reduction of ultimate capacity recorded at about 3.5% as shear stud spacing increased from 75 mm to 150 mm.

The concrete-steel slip for all girders illustrated in Fig. 22. Girder with 150 mm shear stud spacing exceeded the limiting slip value of 1.33 mm according to Euro code specifications (2005). For girders with 75 mm and 120 mm shear stud spacing, the slip is within the limiting value. The study shows that for full composite shear connection level at the negative moment region, a stress level of 0.35 of the ultimate strength for CFRP prescribed.
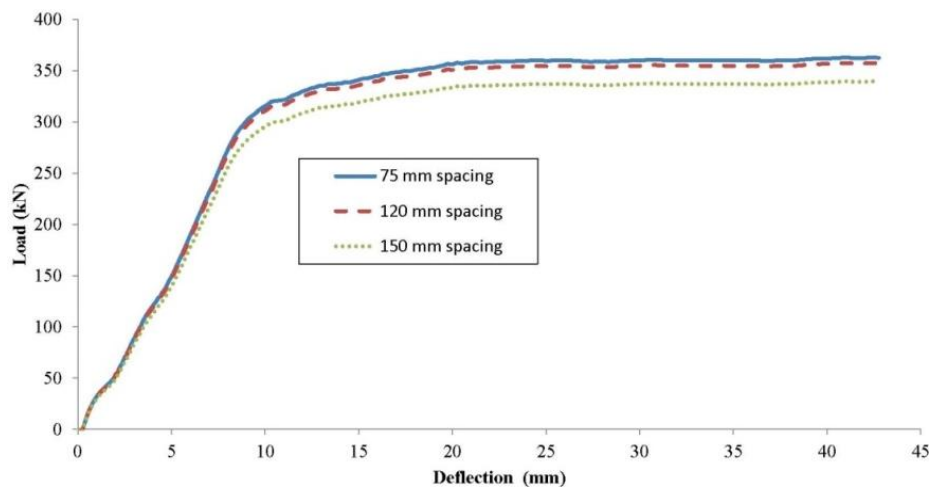

Fig. 21 Load-deflection curves for girders with variable shear stud spacing at negative moment
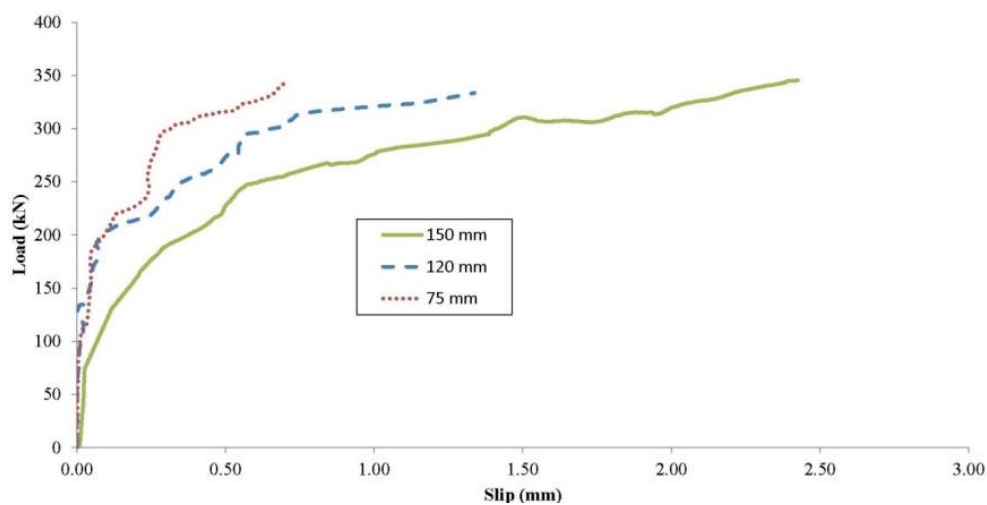

Fig. 22 Load-slip curves of girders with different shear stud spacing

10. Conclusions

A numerical investigation of continuous composite steel girders with CFRP sheets bonded to the top of concrete slab at the negative moment region, supported by a companion experimental study, carried out using an appropriate FE model developed in ABAQUS environment. The developed FE model used in a parametric study has shed light on two critical requirements of such a design namely, thickness and length of CFRP and the shear connectors within the negative moment region for static loads. Based on the findings of the work, the following conclusions may be drawn:

(1) The proposed finite element modelling of a continuous composite steel girder reinforced with CFRP sheets at the negative moment zone using a plastic-damage constitutive law has demonstrated its robustness in predicting the structural behaviour, failure mode and capacity of the composite girder under static loads.

(2) As the structural behaviour and load-carrying capacity are dependent upon the thickness of CFRP used at the negative moment region, the thickness should be judiciously determined to achieve the desired behavioural state to reach full capacity of steel-concrete section at positive and negative moment regions. The developed FE model shown to be capable of an optimal search for the appropriate thickness of CFRP, with minimum compromise in the ductility of the strengthened composite girder.

(3) CFRP sheet should cover the entire length of the negative moment region with a development length of at least 150 mm as recommended by ACI specifications. Influence of de-bonding of the CFRP on the load carrying capacity has been determined using the FEM parametric study module.

(4) The number of shear connectors required to provide the full composite action at the negative moment region calculated to provide shear resistance to the combined longitudinal tensile force due to steel reinforcement yielding and that in the CFRP corresponding to about 35% of its ultimate tensile strength.

Acknowledgments

References

ACI Committee (2008), American Concrete Institute, and International Organization for Standardization. "Building code requirements for structural concrete (ACI 318-08) and commentary", American Concrete Institute.

Ashour, A.F., El-Refaie, S.A. and Garrity, S.W. (2004), "Flexural strengthening of RC continuous beams using CFRP laminates", *Cement Concrete Compos.*, **26**(7), 765-775.

Basu, P.K., Sharif, A.M. and Ahmed, N.U. (1987a), "Partially pre-stressed continuous composite beams. I", *J. Struct. Eng.*, **113**(9), 1909-1925.

Basu, P.K., Sharif, A.M. and Ahmed, N.U. (1987b), "Partially pre-stressed composite beams. II", *J. Struct. Eng.*, **113**(9), 1926-1938.

Bilotta, A. (2010), "Behavior of FRP-to-concrete interface: Theoretical models and experimental

results", Doctoral Dissertation; Universitàdegli Studi di Napoli Federico II, Italy.

Chen, S., Wang, X. and Jia, Y. (2009), "A comparative study of continuous steel–concrete composite beams pre-stressed with external tendons: Experimental investigation", *J. Construct. Steel Res.*, **65**(7), 1480-1489.

Dai, J.G., Gao, W.Y. and Teng, J.G. (2014), "Finite element modeling of insulated FRP strengthening RC beams exposed to fire", *J. Compos. Construct.*, **19**(2), 04014046.

Dundar, C., Tanrikulu, A.K. and Frosch, R.J. (2015), "Prediction of load-deflection behavior of multi-span FRP and steel reinforced beams", *Compos. Struct.*, **132**, 680-693.

Fang, G., Wang, J., Li, S. and Zhang, S. (2016), "Dynamic characteristics analysis of partial-interaction composite continuous beams", *Steel Compos. Struct.*, *Int. J.*, **21**(1), 195-216.

Grace, N.F., Soliman, A.K., Abdel-Sayed, G. and Saleh, K.R. (1999), "Strengthening of continuous beams using fiber reinforced polymer laminates", *ACI Special Publication*, p. 188.

Hawileh, R.A., Naser, M.Z. and Abdalla, J.A. (2013), "Finite element simulation of reinforced concrete beams externally strengthened with short-length CFRP plates", *Compos. Part B*: *Eng.*, **45**(1), 1722-1730.

Joo, H.S., Moon, J., Sung, I.H. and Lee, H.E. (2015), "Moment redistribution of continuous composite I-girder with high strength steel", *Steel Compos. Struct.*, *Int. J.*, **18**(4), 873-887.

Lee, J. and Fenves, G.L. (1998), "Plastic-damage model for cyclic loading of concrete structures", *J. Eng. Mech.*, **124**(8), 892-900.

Lou, T., Lopes, S.M. and Lopes, A.V. (2015), "Neutral axis depth and moment redistribution in FRP and steel reinforced concrete continuous beams", *Compos. Part B*: *Eng.*, **70**, 44-52.

Lou, T., Lopes, S.M. and Lopes, A.V. (2015), "A comparative study of continuous beams prestressed with bonded FRP and steel tendons", *Compos. Struct.*, **124**, 100-110.

Lubliner, J., Oliver, J., Oller, S. and Onate, E. (1989), "A plastic-damage model for concrete", *Int. J. Solid. Struct.*, **25**(3), 299-326.

Malik,,P.K. (1993), *Fiber-Reinforced Composites. Materials, Manufacturing and Design*, (2nd Ed.), CRC.

Nie, J., Tao, M., Cai, C.S. and Li, S. (2011), "Analytical and numerical modeling of pre-stressed continuous steel-concrete composite beams", *J. Struct. Eng.*, **137**(12), 1405-1418.

Sharif, A., Samaaneh, M., Azad, A. and Baluch, M. (2015), "Use of CFRP to maintain composite action for continuous steel-concrete composite girders", *J. Compos. Construct.*,
DOI: 10.1061/ (ASCE) CC.1943-5614.0000645, 040150881-10.

Topkaya, C., Yura, J.A. and Williamson, E.B. (2004), "Composite shear stud strength at early concrete ages", *J. Struct. Eng.*, **130**(6), 952-960.

Tauris, M.J. (2009), "Stress analysis of a fiber reinforced-polymer matrix orthotropic plate with an elliptical hole", Doctoral Dissertation; Resselaer Polytechnic Institute.

URL (2016), http://www.fosroc.com/

Version, A.B.A.Q.U.S. 6.13-1 (2013), User's Manual, ABAQUS.

CC